Monitoring restored tropical forest diversity and structure through UAV-borne hyperspectral and lidar fusion

Danilo Roberti Alves de Almeida [a,b,*], Eben North Broadbent [b], Matheus Pinheiro Ferreira [c], Paula Meli [d], Angelica Maria Almeyda Zambrano [e], Eric Bastos Gorgens [f], Angelica Faria Resende [a], Catherine Torres de Almeida [a], Cibele Hummel do Amaral [g], Ana Paula Dalla Corte [h], Carlos Alberto Silva [i,j], João P. Romanelli [a], Gabriel Atticciati Prata [b], Daniel de Almeida Papa [k], Scott C. Stark [l], Ruben Valbuena [m], Bruce Walker Nelson [n], Joannes Guillemot [a,o,p], Jean-Baptiste Féret [q], Robin Chazdon [r], Pedro H.S. Brancalion [a]

[a] Department of Forest Sciences, "Luiz de Queiroz" College of Agriculture, University of São Paulo (USP/ESALQ), Piracicaba, SP, Brazil
[b] Spatial Ecology and Conservation Lab, School of Forest Resources and Conservation, University of Florida, Gainesville, FL, USA
[c] Cartographic Engineering Department, Military Institute of Engineering (IME), Rio de Janeiro, RJ, Brazil
[d] Landscape Ecology and Conservation Lab (LEPCON), Universidad de La Frontera, Temuco, Chile
[e] Spatial Ecology and Conservation (SPEC) Lab, Center for Latin American Studies, University of Florida, Gainesville, FL, USA
[f] Department of Forestry, Federal University of Jequitinhonha e Mucuri Valleys (UFVJM), Diamantina, Minas Gerais, Brazil
[g] Department of Forest Engineering, Federal University of Viçosa, Viçosa, Minas Gerais, Brazil
[h] Department of Forest Engineering, Federal University of Paraná, Curitiba, Brazil
[i] School of Forest, Fisheries and Geomatics Sciences, University of Florida, Gainesville, FL, USA
[j] Department of Geographical Sciences, University of Maryland, College Park, USA
[k] Embrapa Acre, Rio Branco, Acre, Brazil
[l] Department of Forestry, Michigan State University, East Lansing, MI, USA
[m] School of Natural Sciences, Bangor University, Bangor, UK
[n] National Institute for Amazon Research (INPA), Manaus, AM, Brazil
[o] CIRAD, UMR Eco&Sols, F-34398 Montpellier, France
[p] Eco&Sols, Univ Montpellier, CIRAD, INRAE, Institut Agro, IRD, Montpellier, France
[q] TETIS, INRAE, AgroParisTech, CIRAD, CNRS, Université Montpellier, Montpellier, France
[r] Tropical Forests and People Research Centre, University of the Sunshine Coast, Sippy Downs, QLD 4556, Australia

ARTICLE INFO

ABSTRACT

Remote sensors, onboard orbital platforms, aircraft, or unmanned aerial vehicles (UAVs) have emerged as a promising technology to enhance our understanding of changes in ecosystem composition, structure, and function of forests, offering multi-scale monitoring of forest restoration. UAV systems can generate high-resolution images that provide accurate information on forest ecosystems to aid decision-making in restoration projects. However, UAV technological advances have outpaced practical application; thus, we explored combining UAV-borne lidar and hyperspectral data to evaluate the diversity and structure of restoration plantings. We developed novel analytical approaches to assess twelve 13-year-old restoration plots experimentally established with 20, 60 or 120 native tree species in the Brazilian Atlantic Forest. We assessed (1) the congruence and complementarity of lidar and hyperspectral-derived variables, (2) their ability to distinguish tree richness levels and (3) their ability to predict aboveground biomass (AGB). We analyzed three structural attributes derived from lidar data—canopy height, leaf area index (LAI), and understory LAI—and eighteen variables derived from hyperspectral data—15 vegetation indices (VIs), two components of the minimum noise fraction (related to spectral composition) and the spectral angle (related to spectral variability). We found that VIs were positively correlated with LAI for low LAI values, but stabilized for LAI greater than 2 m^2/m^2. LAI and structural VIs increased with increasing species richness, and hyperspectral variability was significantly related to species richness. While lidar-derived canopy height better predicted AGB than hyperspectral-derived VIs, it was the

fusion of UAV-borne hyperspectral and lidar data that allowed effective co-monitoring of both forest structural attributes and tree diversity in restoration plantings. Furthermore, considering lidar and hyperspectral data together more broadly supported the expectations of biodiversity theory, showing that diversity enhanced biomass capture and canopy functional attributes in restoration. The use of UAV-borne remote sensors can play an essential role during the UN Decade of Ecosystem Restoration, which requires detailed forest monitoring on an unprecedented scale.

1. Introduction

An ambitious restoration agenda has been set to increase forest cover in deforested and degraded landscapes, to improve their multi-functionality and capacity to provide essential ecosystem services, such as maintaining biodiversity, water supply and carbon storage (Erbaugh and Oldekop, 2018). Forest monitoring will play a crucial role to track the success of these goals and also support adaptive management (Brancalion and Holl, 2020; Fagan et al., 2020), given the widespread failures in ecosystem restoration and the unprecedented scale of restoration pledges (Versluijs et al., 2019; Chagas et al., 2021). Currently, there is a pressing need to develop social collaborative and effective technologies for monitoring ecosystem recovery over large areas (hundreds to millions of hectares) using multiple key ecological indicators (Guariguata and Evans, 2020; Höhl et al., 2020). Remote sensors onboard orbital platforms, aircraft, or unmanned aerial vehicles (UAVs) have emerged as promising technologies to upscale forest restoration monitoring. Particularly, UAV systems can generate high-resolution images that provide accurate information on forest stands with or without the need for ground-based data (e.g., calibration or validation) to estimate important forest attributes such as the number of trees, aboveground biomass, or canopy openness (Almeida et al., 2020a; Kotivuori et al., 2020; Ferreira et al., 2020).

Accurate methods to estimate forest attributes to support decision-making are required for the effective remote monitoring of forests undergoing restoration (Almeida et al., 2019a). For example, forest cover, biomass stock and tree species diversity vary along forest successional sequences and are commonly employed to monitor forest restoration (Wortley et al., 2013). To this aim, multispectral sensors have proven useful, offering estimates of these critical variables. However, a high leaf area index (LAI) saturates most vegetation indices (VIs) derived from remote sensing (Turner et al., 1999). This saturation complicates their use to monitor structural attributes (such as aboveground biomass - AGB) in high-LAI tropical forests, which account for a large portion of global restoration commitments (Timothy et al., 2016; Crouzeilles et al., 2019). On the other hand, the light detection and ranging (lidar) sensor has been hailed as a promising technology for retrieving forest canopy structural attributes, regardless of canopy leaf area density. Lidar enables the estimation of canopy structural attributes with high precision and accuracy, such as vegetation density in the understory, LAI, tree height, the identification and measurement of forest gaps, and AGB (Almeida et al., 2019b; da Costa et al., 2020; Valbuena et al., 2020; Dalagnol et al., 2021). On the other hand, lidar technology is of limited use for assessing tree species diversity, for which hyperspectral has shown greater potential (Asner and Martin, 2009).

Assessing the different facets of forest diversity, such as tree richness, functional diversity, and composition, is one of the most important but challenging modern remote sensing tasks (Asner, 2015). With lidar, one approach is to use canopy structural attributes as predictive variables for indirectly estimating tree species diversity (Hernández-Stefanoni et al., 2014; Ali et al., 2019; De Cáceres et al., 2019; Adhikari et al., 2020). Notably, a more species-rich forest is expected to have a more heterogeneous and complex canopy structure (Zellweger et al., 2019; Mensah et al., 2020). Secondary forests with higher biomass are expected to have reached a later stage of succession, supporting more

tree species (Gamfeldt et al., 2013; Lasky et al., 2014; Finegan et al., 2015; Poorter et al., 2015). However, structure–richness relationships are not ubiquitous and depend on a wide range of factors, such as forest type, management, use and disturbance history. Consequently, the lidar approach has so far demonstrated a limited ability for local scale prediction of species richness, especially in hyper-diverse tropical biomes (Marselis et al., 2020; Almeida et al., 2019a; Valbuena et al., 2020).

Hyperspectral imaging (HSI) has a significant potential for estimating or measuring taxonomical and functional diversity of highly diverse tropical forests (Féret and Asner, 2014; Vaglio Laurin et al., 2016; Durán et al. 2019). HSI measures reflected radiation from the forest canopy over hundreds of narrow spectral bands (or channels) within the visible- to short-wave infrared wavelength range (VSWIR, 400–2500 nm). The rationale for using hyperspectral sensors to discriminate species-richness is that each species (or group of species) has specific combinations of spectral features. These include absorption by specific chemical constituents of leaves and non-photosynthetic elements and scattering driven by vegetation structure at different scales, such as leaf anatomy, leaf area index, leaf angle distribution function (Ferreira et al., 2016). However, this combination of spectral traits does not necessarily result in a unique species-specific spectral identity (and thus perfect discrimination among species), as significant intraspecific variability in spectral traits was evidenced (Amaral et al., 2018; Camarretta et al., 2020). For example, a single species' spectral characteristics can vary widely depending on environmental variables (e.g., water availability) or species and community attributes (e.g., leaf amount and leaf age) (Yan et al., 2018; Ferreira et al., 2019; Gonçalves et al., 2020). Another rationale is that the spectral heterogeneity is related to tree species diversity and composition (Rocchini et al., 2010; Féret and Asner, 2014; Asner et al., 2017; Laliberté et al., 2020). HSI also enables linking canopy reflectance to biophysical and chemical properties using various approaches, including narrow-band vegetation indices, which are designed to be used as proxies for both structural (e. g., vegetation density) and physiological (e.g., leaf chemical composition and water stress) properties (Zhao et al., 2018).

Using HSI data to study species diversity or the retrieval of canopy chemical properties is still challenging, particularly in tropical ecosystems due to their high biodiversity and structural complexity (Feret and Asner, 2013). HSI data acquisition with airborne surveys is usually costly, planning intensive, and may be operationally prohibitive in places with poor infrastructure and resources, such as in some tropical forest regions. Conversely, restoration practitioners face the challenges of monitoring tree diversity in tropical forest regions (Crouzeilles et al., 2019), given the difficulty of properly identifying hundreds of tree species and the reduced accessibility of restoration areas for forest inventories (Keil and Chase, 2019). As restoration programs are usually composed of several small to mid-size polygons scattered across large and heterogeneous areas, airborne surveys are less viable.

Recent technological developments have allowed for manufacturing UAV-compatible HSI sensors, a promising approach to mainstreaming the common use of HSI in tropical forest restoration monitoring. UAVs are a technological frontier of remote sensing data acquisition and may constitute an alternative to high-cost airborne hyperspectral and lidar campaigns. The use of UAV-borne remote sensors, both lidar and HSI, nonetheless presents pros and cons. The main advantage is the higher

spatial resolution. Point cloud density from airborne lidar usually ranges between 0.4 and 30 points per m² (ppm²), whereas UAV lidar acquisitions can reach 100–1000 ppm² (d'Oliveira et al., 2020; Prata et al., 2020). The high point density increases the accuracy of estimating structural parameters, such as vertical profiles of leaf area density (Almeida et al., 2019a). It can even allow the individualization of trees and measurement of stem volume in open-canopy forests such as eucalyptus plantations (Dalla Corte et al., 2020) and temperate forests (Krůček et al., 2020). For UAV-HSI, the centimetric resolution of the pixels allows a better characterization of target objects, detecting vegetation-free patches, removing background contribution, and capturing the spectral variability within and among crowns. Conversely, flight instability of the UAV, changing view and illumination geometry and changing sky conditions make the use of these images challenging. HSI reflectance retrievals from UAVs require a matched incident radiance HSI sensor and non-trivial pre-processing steps, including corrections for bidirectional reflectance distribution function (BRDF) and atmospheric effects (Jia et al., 2020).

To date, few investigations have assessed the potential of UAV-lidar-HSI systems in tropical forest monitoring. Sankey et al. (2017) and Lin et al. (2019) used UAV-lidar-HSI systems to monitor semi-arid and pine forests, respectively. Here, we explored the fusion of UAV-borne lidar and hyperspectral data to remotely access the structure and diversity of restored tropical forests. We developed a novel analytical approach for a mixed-species, 13-year-old restoration plantation experimentally established with 20, 60, and 120 native tree species in the Brazilian Atlantic Forest. Specifically, we assessed (1) the congruence of lidar and hyperspectral variables, (2) their usefulness to distinguish tree species richness levels, and (3) their ability to predict aboveground biomass. Our work goes well beyond traditional measurements based on sampling plots, providing high-accuracy and precision information for upscaling field variables to satellite-based hyperspectral and lidar observations, representing an effective strategy for large-scale forest restoration monitoring during the United Nations Decade on Ecosystem Restoration (2021−2030).

2. Methods

2.1. Experimental site and field data

We used an experimental mixed-species restoration plantation with three diversity levels to explore the potential and limitations of fusing UAV-borne lidar and hyperspectral data to assess structure and diversity. The experimental plots were established in May 2006 in Anhembi-SP, southeastern Brazil, in a completely randomized design with 20, 60, and 120 native tree species (hereafter sp.), each with four replicates, in 45 × 48 m plots (Fig. 1). The area was previously covered by pastures, with no regeneration of native tree species. Tree seedlings were randomly planted with 3 × 1.5 m spacing and ensuring a homogeneous density across species. The species pool present in the treatments with the lowest richness was contained in the treatments with higher richness, i.e., species of the treatment of 20 species are contained in the treatment of 60 species, which are also contained in the treatment of 120 species. Extensive information on the study site and experiment is provided by Duarte et al. (2021). Due to the low coverage of HSI in one plot, the treatment of 120 species had only three replicates for the analysis using HSI data. Forest inventory field data were collected in November 2019, when the plantation was 13.5 years old. At this time, 58 and 114 species had survived in the 60- and 120 species treatments, respectively. For all living stems, we identified the tree species in this inventory, measured diameter 30 cm above the ground and measured total height. We used the allometric equation developed by Ferez et al. (2015) for a neighboring restoration plantation to estimate aboveground woody biomass of each individual (Eq. (1)). Wood densities were obtained for all tree species based on wood discs (cross-sections from the stem) sampled in destructive plots established, using three individuals per species (see Ferez, 2012 for more details).

$$ln(AGB_w) = 6.039 + 0.945ln(SA) + 0.961ln(Ht) + 1.002\ ln(\rho) \tag{1}$$

where: AGBw = Aboveground woody biomass (Mg/ha); SA: sectional area of the stem (m²); Ht: total height (m); ρ = wood density (g/cm³).
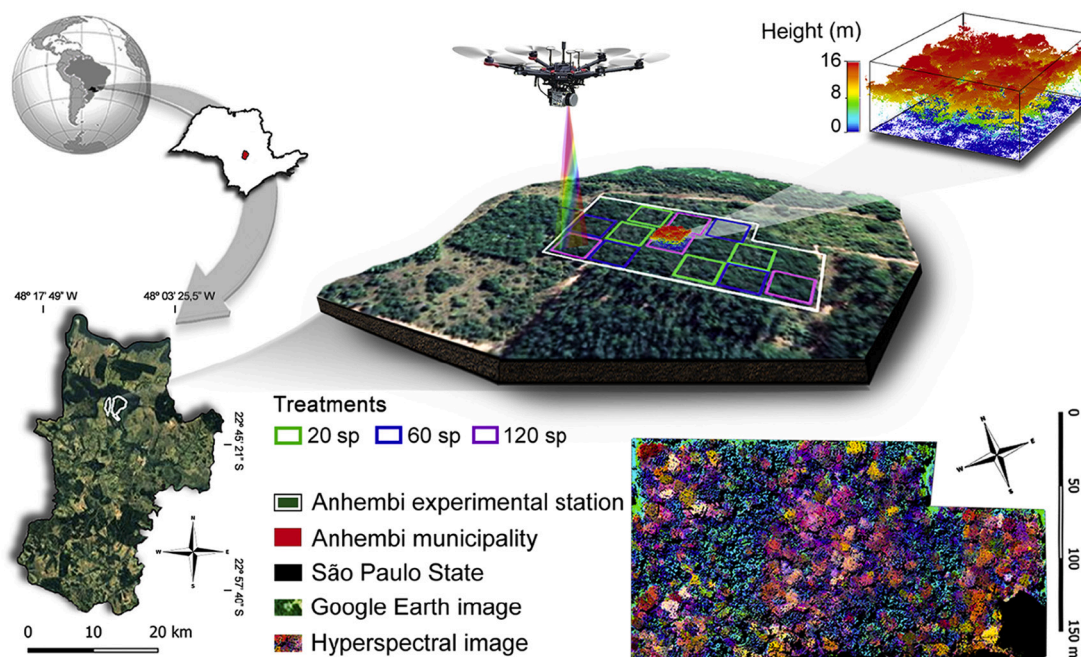

Fig. 1. Study area and plot designs. Left) site location; upper right) sample design and lidar point cloud example of one plot; bottom right) hyperspectral image colored by a false RGB composition using the first components from the minimum noise fraction transformation.

2.2. UAV-borne lidar and hyperspectral data

Data were collected using the GatorEye Unmanned Flying Laboratory, consisting of a hardware system with custom algorithm workflows incorporating lidar, hyperspectral, thermal, and visual (RGB) sensors. The hardware and processing workflows are described in detail in the GatorEye overview manuscript (Broadbent et al., 2021) available at www.gatoreye.org. The data is also available under the section "2019 Brazil Sao Paulo State August/082819".

The system uses a DJI Matrice 600 Pro hexacopter platform, with mission planning conducted using Universal Ground Control Station (UGCS) software. GNSS base station data are collected within 3 km of data collection areas, then post-processed online via the Trimble CenterPoint RTX platform, providing typically <2 cm 3D uncertainty within a 2-h collection period (and < 0.25 cm within 4+ hour collections). The computational sensor core is based on a Phoenix Ultra Scout, a Novatel STIM 300 IMU tactical grade and differential GNSS system. Integrated into this is a (a) Velodyne VLP-32c Ultra Puck LiDAR sensor, (b) Nano VNIR Hyperspectral Headwall sensor (640 pixels × 270 spectral bands in a 100-hertz line scan approach), (c) high-resolution RGB camera, (d) radiometric thermal camera, and (e) time-synchronized downwelling hyperspectral Ocean Optics Flame (upward viewing spectrometer, 400-1025 nm wavelength range, and 1.70 nm spectral resolution) (Fig. S1). See Broadbent et al. (2021) for more details.

The Velodyne Ultra Puck sensor features 32 individuals 905 nm lasers, situated to provide a 360° horizontal (cross-track) and 40° vertical (along-track) field of view. The Ultra Puck fires 600,000 times per second, recording for each pulse the strongest and the last (dual) return, for a theoretical points/s of 1,200,000 at a range of up to 200 m. The Headwall Photonics Nano VNIR 270 spectral band lab-calibrated radiance hyperspectral sensor acquires 1400 spectral bands from 400 to 1000 nm every 0.5 s and allows conversion of radiance to reflectance by ratioing with the spectral bands most similar in wavelength from the upward-facing Ocean Optics Flame sensor (Broadbent et al., 2021).

The GatorEye overflew the experimental area 27–30 Aug of 2019 at approximately solar noon at an aboveground mean altitude of 100 m. The local solar zenith angle was 32 degrees at solar noon (based on the date 28 Aug 2019, lat, long = −22.75, −48.11). Four flight lines were acquired to cover the majority of plots. The speed was 12–14 m/s, resulting in a forward pitch of approximately 12 degrees during flight. Acquisitions were performed under clear sky conditions with no atmospheric haze. The specific lidar and hyperspectral GatorEye deliverables used in this study were: (a) the Canopy Height Model (CHM), (b) the cleaned lidar point cloud, and (c) the 'reflectance-calibrated hyperspectral shade-filtered orthomosaic' (e.g., HSI image).

Lidar flight lines were processed to standard products using the GatorEye Multi-scalar Post-Processing workflow – using the software Lastools (Isenburg, 2020) and "lidR" R package (Roussel and Auty, 2019). This procedure automatically merges flight lines, classifies ground points and removes noise – to generate the cleaned point clouds and the rasters DTM (digital terrain model), DSM (digital surface model) and CHM. More details are given in Almeida et al. (2019b, 2020a), Almeida et al. (2020b). The point density of the final lidar point cloud was 360 ± 137 (mean $\pm$ *SD*) ppm^2, of which 80.4% were first returns.

Hyperspectral data were processed in three steps. (1) The non-orthorectified time-synchronized lab-calibrated radiance data from the downward-facing boresighted Nano hyperspectral camera was projected onto the DSM from the lens using a ray-tracing algorithm. (2) The radiance bands were then converted to reflectance using the also time-synchronized and lab-calibrated upward-facing Flame hyperspectral irradiance sensor. (3) The shade was removed through a separate process where solar geometry was calculated and then applied, through a ray tracing algorithm (Broadbent et al., 2021), to map portions of the DSM to be either in full sunlight or in the shade at the moment of data acquisition. Shaded pixels were masked in the final hyperspectral reflectance orthomosaic. Hyperspectral images are orthorectified onto

the lidar derived digital surface models using a custom ray tracing workflow (Broadbent et al., 2021). The spatial resolution of the final HSI image was 0.20 m. We performed additional filtering on the hyperspectral data using a 0.20 m moving window filter across the CHM to remove pixels with a height below four meters. This filtering enabled us to restrict the spectral data to vegetation targets when estimating tree species compositional values versus being dominated by the ground level exposed soil spectra which greatly differ from vegetation.

The bidirectional reflectance distribution function (BRDF) describes the variations in reflectance or radiance intensity measured by a sensor as a function of (1) the angle of separation of two vectors - view and illumination - and of (2) forward-scatter (viewing toward the sun) and backscatter (sun behind the viewer). In remotely sensed imagery, BRDF significantly impacts the retrieval of biophysical surface properties (Wanner et al., 1995). We corrected the HSI orthomosaic for BRDF effects using a kernel-driven approach. More details can be found in the Supplementary Material.

2.3. Data processing and analysis

Post-deliverables data processing was performed in the R environment (R Core Team, 2020). Three structural attributes were derived from lidar data: canopy height, leaf area index - LAI, and leaf area index in the understory - LAI.under. (Table 1). At the plot level, we calculated the mean canopy height and its heterogeneity (standard deviation). The canopy height was obtained directly from the CHM (0.20 m resolution). To calculate canopy height, the cloud pulse density was not filtered to a standard density, ensuring the highest accuracy. Nonetheless, Silva et al. (2017) have shown that the accuracy of canopy height estimate in Amazon forests stabilizes when pulse density reaches 4 ppm^2. The LAI (1 m resolution) was calculated from the leaf area density (LAD) estimated using the *lad.voxels* function from the "leafR" package (Almeida et al., 2019c). The LAI is the sum of the entire LAD vertical profile, and the LAI understory is the sum of the LAD vertical profile between 1 and 5 m in height. To improve the accuracy of the LAD estimates and remove lidar pulse density bias, the normalized lidar cloud was filtered to first returns only and then homogenized to 30 ppm^2 before the LAD calculation. Almeida et al. (2019a) found that higher pulse densities result in higher LAI estimates in tropical forests. While this bias is small when pulse densities exceed 20 ppm^2, for all LAI and LAD estimates we elected to standardize to 30 ppm^2 using a homogenizing filter. The method used to estimate the LAD uses the MacArthur-Horn equation (MacArthur and Horn, 1969) and is based on the Beer-Lambert law, i.e., the attenuation of the energy transmission rate (lidar pulses) between the canopy vertical strata. See Almeida et al. (2019a) for more details.

A total of 18 variables derived from HSI data were calculated (Table 1): 15 vegetation indices (VIs), the first two components of the minimum noise fraction (MNF) transformation (related to spectral composition), and the spectral angle (related to spectral variability). VIs were divided into four categories: (i) Structural, (ii) Chlorophyll, (iii) Anthocyanin / Carotenoid, and (iv) Physiology. MNF is a linear transformation of the original HSI data that applies two cascaded PCA and maximizes the signal/noise ratio (Green et al., 1988). We performed MNF using ENVI software version 5.3.

To assess if species diversity is related to canopy spectral diversity, we computed the spectral angle between all pairwise combinations of the pixels of each treatment. The spectral angle (θ) is a suitable measure of the spectral variability (Richter et al., 2016; Ferreira et al., 2018), and was computed as follows, according to Price (1994):

$$\theta = cos^{-1}\left(\frac{\int_{\lambda_a}^{\lambda_b} X(\lambda)Y(\lambda)d\lambda}{\left[\int_{\lambda_a}^{\lambda_b} X(\lambda)^2 d\lambda\right]^{\frac{1}{2}} \left[\int_{\lambda_a}^{\lambda_b} Y(\lambda)^2 d\lambda\right]^{\frac{1}{2}}} \right) \quad (2)$$

where θ is the spectral angle, measured in radians, between the spectral reflectance of the pixel *X* and the pixel *Y* in the spectral interval λ_a to λ_b,

Table 1
Variables and their respective descriptions and references. "ρ" indicates reflectance of a hyperspectral band, followed by its wavelength center in nanometers.

Variable	Description	Reference
Field-derived		
Aboveground biomass - AGB (Kg)	Eq. (1)	Ferez et al., 2015
Canopy structural attribute (Lidar-derived)		
Canopy height - CH (m)	Mean of canopy height model	Almeida et al., 2019b
Leaf area index - LAI	Sum of leaf area density profile	Almeida et al., 2019a
LAI understory - LAI.under	Sum of leaf area density profile (1–5 m)	Almeida et al., 2019b
Structural VIs (HSI-derived)		
Vegetation Atmospherically Resistant Index (VARI)	$(\rho557 - \rho643) / (\rho557 + \rho643 - \rho465)$	Gitelson et al., 2002
Simple Ratio (SR)	$\rho865 / \rho672$	Jordan, 1969
Normalized Difference Vegetation Index (NDVI)	$(\rho865 - \rho672) / (\rho865 + \rho672)$	Rouse et al., 1974
Enhanced Vegetation Index (EVI)	$2.5 \times ((\rho865 - \rho672) / (\rho865 + 6 \times \rho672 - 7.5 \times \rho464 + 1))$	Huete et al., 2002
Chorophyll VIs (HSI-derived)		
Structurally Insensitive Pigment Index (SIPI)	$(\rho800 - \rho445) / (\rho800 + \rho680)$	Peñuelas et al., 1995
Chlorophyll Absorption in Reflectance Index (CARI)	$(\rho700 - \rho670) - 0.2 \times (\rho700 - \rho550)$	Kim (1994)
Chlorophyll Red-Edge Index (CI.rededge)	$\rho851 / \rho730 - 1$	Gitelson et al., 2006
Chlorophyll Green Index (CI.green)	$\rho730 / \rho531 - 1$	Gitelson et al., 2006
Anthocyanin VIs (HSI-derived)		
Modified Anthocyanin Reflectance Index (mARI)	$(1 / \rho551) - (1 / \rho701)$	Gitelson et al., 2006
Anthocyanin Content Index (ACI)	$\rho531 / \rho941$	van den Berg and Perkins, 2005
Carotenoid VI (HSI-derived)		
Carotenoid Reflectance Index (CRI)	$(1 / \rho511) - (1 / \rho551)$	Gitelson et al., 2007
Physiology VIs (HSI-derived)		
Photochemical Reflectance Index (PRI)	$(\rho531 - \rho571) / (\rho531 + \rho571))$	Gamon et al., 1997
Red-edge Vegetation Stress Index (RVSI)	$(\rho712 + \rho753) / 2 - \rho733$	Merton and Huntington, 2021
Red edge position (REP)	Max first derivative: 680–750 nm	Horler et al., 1983
Water Band index (WBI)	$\rho900 / \rho X970$	Peñuelas et al., 1997
Spectral composition (HSI-derived)		
MNF.1	First component of minimal noise fraction	Green et al., 1988
MNF.2	Second component of minimal noise fraction	Green et al., 1988
Spectral heterogeneity (HSI-derived)		
Spectral angle	Eq. (2)	Price, 1994

i.e., 400 to 1000 nm. The spectral angle was computed with sunlit foliated canopy pixels that were selected using NDVI >0.8 and canopy height > 4 m. We used sunlit foliated canopy pixels to avoid the influence of non-photosynthetic canopy elements (e.g., branches) in the quantification of spectral diversity. Non-photosynthetic vegetation causes variations in the spectral amplitude, that is, brightness differences that may increase the spectral variability even if the spectral shapes were the same.

We used Spearman's correlation diagram to assess the relationship between the VIs (HSI-derived) and the canopy structural variables (lidar-derived). This analysis was performed at the pixel level (0.20 m resolution). The variables AGB (field-derived) and spectral angle (HSI-derived) were evaluated at the plot level. For comparing the spectral angle, only the highest spectral angles of each plot (percentile 90%)

were considered. This ensures that the test assesses the most significant differences within the plots. To determine the relationship of the variables with the tree species richness levels (treatments), we performed ANOVA and post-hoc Tukey tests (plot-level analysis). For these analyses, we considered the variables' mean value and standard deviation within the plots, and the latter was used to describe the heterogeneity of each variable within plots. Finally, the predictive power of AGB from lidar and HSI variables was evaluated using simple and multiple ordinary least square regressions. To identify and eliminate outliers, we used *t*-tests based on studentized residuals implemented using the function outlier.test in R package "car" (Fox and Weisberg, 2019). The assessment of model accuracy was performed by a leave-one-out cross-validation (LOOCV) procedure (Almeida et al., 2020a). The relationship between the observed and predicted (via LOOCV) values were evaluated by testing their 1:1 correspondence under the null hypothesis that their regression intercept and slope were 0 and 1, respectively (Valbuena et al., 2017).

3. Results

3.1. Variables derived from lidar and HSI

Lidar-derived LAI was significantly correlated with almost all HSI-derived variables at the pixel level (Fig. 2). The structural VIs (HSI-derived) had the highest correlations with LAI ($r > 0.50$, *p*-values <0.05). In general, structural VIs increased between LAI values ranging from 0 to 2, but then saturated (Fig. 3). The canopy height attribute CH (lidar-derived) was significantly correlated with seven HSI-derived variables (Fig. 2), with EVI being the VI variable with the highest correlation ($r = 0.22$, *p*-value = 0.006). The EVI and the other structural VIs all showed a positive correlation with CH for values ranging from 5 to 15 m, but they stabilized or decreased for CH values within 15–20 m (Fig. 3). The lidar-derived understory LAI (LAI.under) showed no significant correlation with any of the HSI-derived variables.

3.2. Distinguishing tree species richness levels

The 20 sp. treatment had lower field-derived AGB (mean ± *SE*, 69.5 ± 10.4 Mg/ha) than the 60 sp. treatment (94.3 ± 9.8 Mg/ha), whereas the 120 sp. treatment had intermediate (88.7 ± 15.6 Mg/ha) AGB and did not differ statistically from the other two treatments (Table 2). However, when changing the significance level to 0.1 (instead of 0.05), the two treatments with the highest species richness (60 and 120 sp.) showed higher AGB than the treatment with the lowest species richness (20 sp.).

The CH (lidar-derived) was higher in the two species-richer treatments (60 and 120 sp.) (Table 2). However, the CH heterogeneity did not significantly differ between richness levels (Table S1, *p*-value = 0.59). The richest treatment had the highest LAI value, and when considering the significance level at 0.1, a significant increase in LAI was verified with the increase in species richness class. The LAI heterogeneity was higher in the two richest treatments (Table S1, p-value <0.001). LAI.under showed no difference among richness levels (Table 2 and Fig. 5). The vertical distribution of the LAD was mono-modal, with a higher concentration of vegetation in the middle layer of the canopy for all three treatments (Fig. 4).

For the HSI-derived VIs, the structural VIs (VARI, SR, NDVI, and EVI) increased with increasing richness (Table 2), and in some of them (VARI and NDVI), the heterogeneity was lower in the 120 sp. treatment (Table S1, *p*-values <0.05). For the VIs related to chlorophyll concentration, SIPI decreased with increasing richness (SIPI is inversely proportional to chlorophyll concentration), while CI.rededge and CI.green increased with increasing species richness. The CARI VI showed no significant difference among richness treatments. For the VIs related to the anthocyanin concentration, the mARI has no significant difference, although its heterogeneity was greater in the richest treatment. ACI was lower in
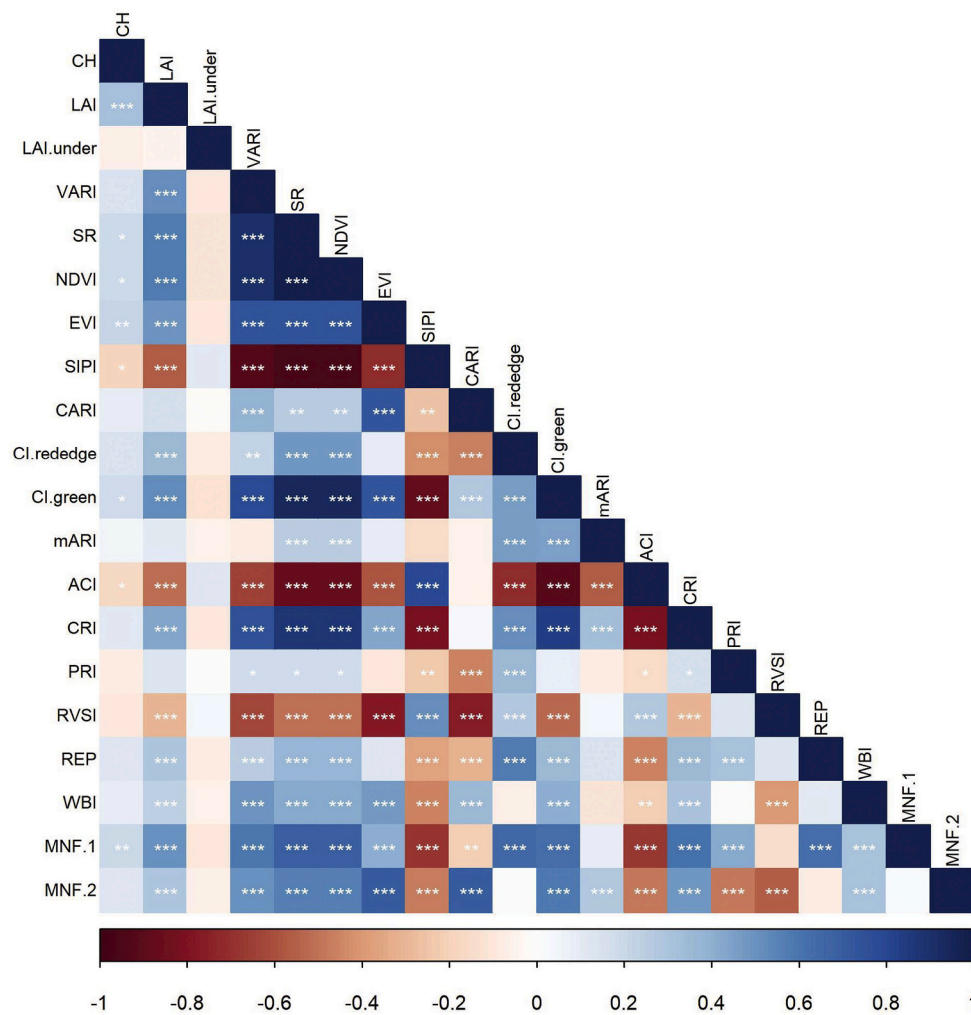
Fig. 2. Spearman's correlation diagram among the lidar- and hyperspectral-derived variables. The correlation values are ranked using a color gradient from −1 to 1, where 0 means no correlation, −1 a strong negative correlation (red color), and one a strong positive correlation (blue color). The *p*-value significance levels are "*" 0.05, "**" 0.01, and "***" 0.001. Acronyms of variables are described in Table 1. (For interpretation of the references to color in this figure legend, the reader is referred to the web version of this article.)
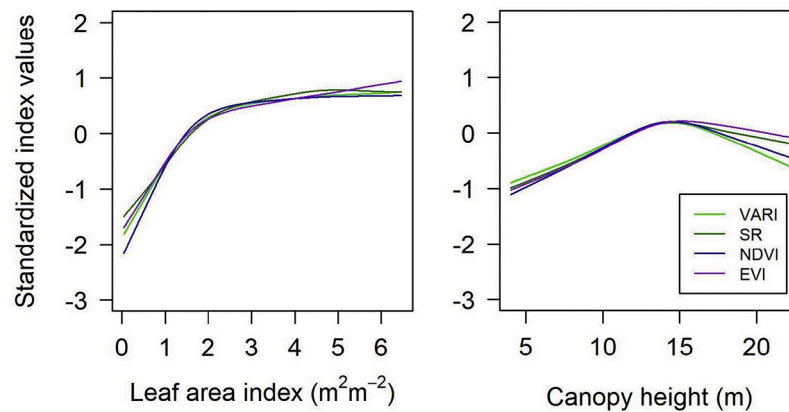

Fig. 3. Standardized hyperspectral-derived structural vegetation indices (Vegetation Atmospherically Resistant Index - VARI, Simple Ratio - SR, Normalized Difference Vegetation Index - NDVI, and Enhanced Vegetation Index - EVI) as a function of lidar-derived leaf area index (LAI) (left) and lidar-derived canopy height (CH) (right). Lines are the smoothed mean of the observations (pixels of 0.20 m resolution).

the lowest richness treatment. The VI related to carotenoid concentration, CRI, was higher in the richest treatment (with a significant gradual increase at the 0.1 significance level).

For the physiological VIs, RVSI decreased with the increase in richness, while the REP showed a directly proportional relationship with the increase in richness. WBI presented no significant difference, and PRI did not show a clear relationship with richness levels. The composition variable MNF.1 increased its mean and heterogeneity proportionally with richness (Table 2 and Table S1). The MNF.2 did not show any significant difference between treatments. Spectral variation increases with increasing richness (Fig. 5). The spectral angle, a proxy for the spectral diversity, showed a significant difference with richness levels

Table 2
Statistical analysis (mean ± *SE*; ANOVA post hoc Tukey) of field, lidar, and hyperspectral (HSI) variables by plot comparing diversity level treatments (20, 60, and 120 sp.). Lidar and hyperspectral variables were summarized by the mean of the pixels (0.20 m resolution). The significant variables were colored green ranging from the lowest (light green) to the highest (dark green) values.

| Type	Variable	Treatment 20sp	Treatment 60sp	Treatment 120sp	p-value
Field	AGB	69.459 ± 10.409 b	94.253 ± 9.736 a	88.698 ± 15.55 ab	0.043
Lidar	CH	10.331 ± 1.029 b	12.77 ± 1.098 a	12.993 ± 0.973 a	0.01
	LAI	1.063 ± 0.149 b	1.711 ± 0.139 b	2.639 ± 0.589 a	0.001
	LAI.under	0.074 ± 0.007	0.092 ± 0.017	0.08 ± 0.014	0.223
Structural	VARI	0.11 ± 0.023 c	0.167 ± 0.016 b	0.248 ± 0.003 a	< 0.001
	SR	7.728 ± 0.882 c	9.931 ± 0.94 b	12.987 ± 0.395 a	< 0.001
	NDVI	0.722 ± 0.024 c	0.776 ± 0.02 b	0.835 ± 0.007 a	< 0.001
	EVI	0.436 ± 0.009 b	0.496 ± 0.03 ab	0.534 ± 0.048 a	0.008
Chlorophyll	SIPI	1.118 ± 0.017 a	1.078 ± 0.012 b	1.042 ± 0.004 c	< 0.001
	CARI	0.027 ± 0.001	0.028 ± 0.002	0.027 ± 0.005	0.612
	CI.rededge	0.504 ± 0.038 b	0.556 ± 0.023 ab	0.622 ± 0.038 a	0.005
	CI.green	3.226 ± 0.179 c	3.719 ± 0.239 b	4.313 ± 0.082 a	< 0.001
Anth/Caro	mARI	1.691 ± 0.079	1.78 ± 0.143	1.798 ± 0.071	0.381
	ACI	0.193 ± 0.014 a	0.166 ± 0.011 b	0.143 ± 0.004 b	0.001
	CRI	12.574 ± 1.672 b	15.327 ± 1.834 b	19.802 ± 2.527 a	0.004
Physiology	PRI	-0.084 ± 0.002 ab	-0.086 ± 0.006 b	-0.071 ± 0.009 a	0.021
	RVSI	-0.009 ± 0.001 a	-0.01 ± 0.001 ab	-0.012 ± 0.001 b	0.032
	REP	715.857 ± 2.854 b	719.913 ± 2.389 ab	723.277 ± 2.091 a	0.014
	WBI	1.232 ± 0.014	1.233 ± 0.015	1.251 ± 0.008	0.169
Hyperspectral variability	MNF.1	-1.568 ± 0.431 b	-0.989 ± 0.187 b	1.125 ± 0.657 a	< 0.001
	MNF.2	-0.608 ± 0.322	0.118 ± 0.82	-0.079 ± 0.972	0.391
	Spectral angle	0.111 ± 0.008	0.122 ± 0.011	0.127 ± 0.004	0.09
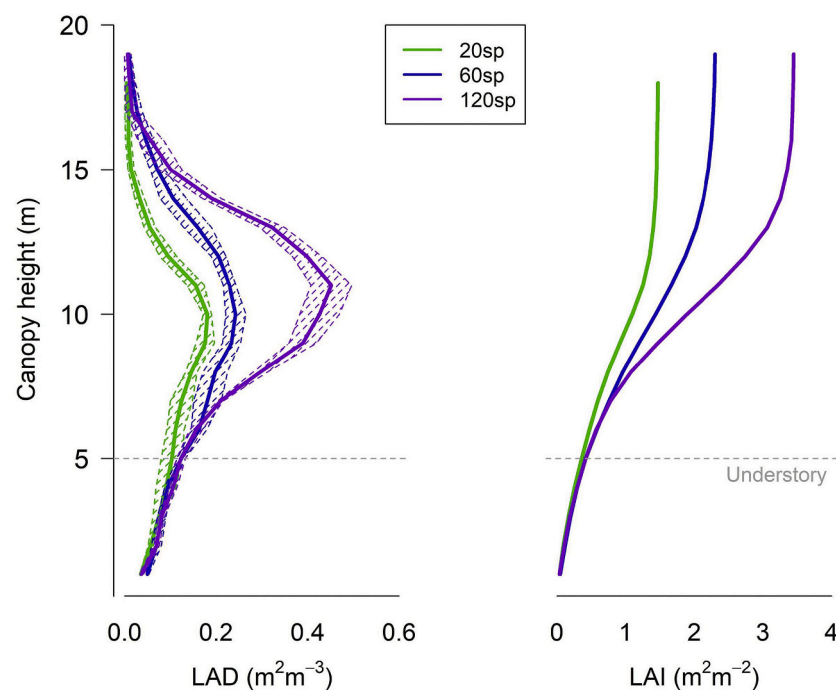
Fig. 4. Mean leaf area density (LAD) profiles (left) and cumulative leaf area (LAI) (right) for the three tree diversity level treatments (20, 60, and 120 sp.). Lines are the plots' mean, and the dashed polygons represent the standard error amplitude.
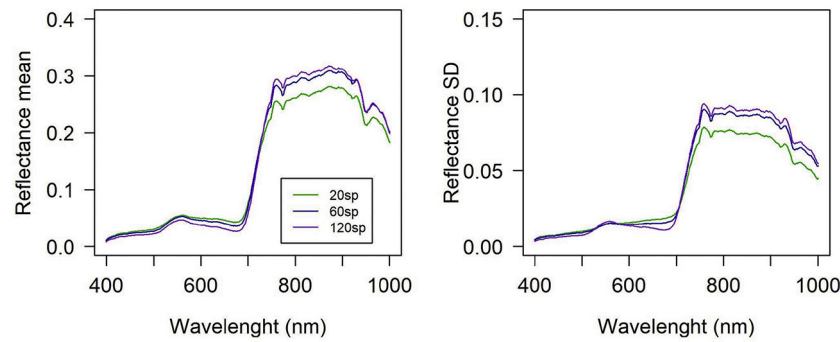
Fig. 5. Mean (left) and standard deviation (*SD*) (right) of reflectance for the three tree richness level treatments (20, 60, and 120 sp.).

only when the significance of 0.1 was considered (*p*-value = 0.09).

3.3. Predicting aboveground biomass

The AGB were significantly correlated ($p < 0.001$) with one lidar-derived variable (CH, r = 0.81), and three HIS-derived VIs (RVSI, r = 0.78; EVI, r = 0.76; and CARI, r = 0.77) (Fig. S2). However, after eliminating an outlier observation, the best AGB predictors were CH (r^2 = 0.82, RMSE = 7.62, relative RMSE = 9.0%), followed by the RVSI (r^2 = 0.75, RMSE = 8.98, relative RMSE = 10.1%) (Fig. 6). Multiple regression models did not provide significant improvements.

4. Discussion

Our UAV-lidar-HSI system showed a strong potential to assess canopy structure, AGB, and tree diversity in tropical forest restoration plots, combining lidar and the VIs derived from HSI. It also helped reveal a suite of canopy differences related to forest structure and ecosystem

function over an experimental biodiversity gradient. This included both bulk properties like height and LAI (from lidar) and physiologically-linked community traits such as EVI 'greenness' (from hyperspectral), consistent with theories about the advantages of higher biodiversity in restoration. To our knowledge, this is the first study to use both lidar and HSI onboard a UAV to monitor tropical forest restoration (but see Vaglio Laurin et al., 2014 for a pioneer attempt in a mature tropical forest).

4.1. Variables derived from lidar and HSI

Almost all HSI variables were significantly correlated with the LAI. In general, VIs including information from the NIR domain (750–850 nm, a spectral region characterized by multiple scattering of foliar tissues) show sensitivity to LAI. However, the VIs tend to saturate for LAI values higher than 2. Only mARI and PRI (which do not use NIR information) did not correlate with LAI. VARI and CRI do not have NIR bands in their equation but nonetheless showed a saturating correlation with LAI. These VIs are related to the photosynthetically active leaf area, with
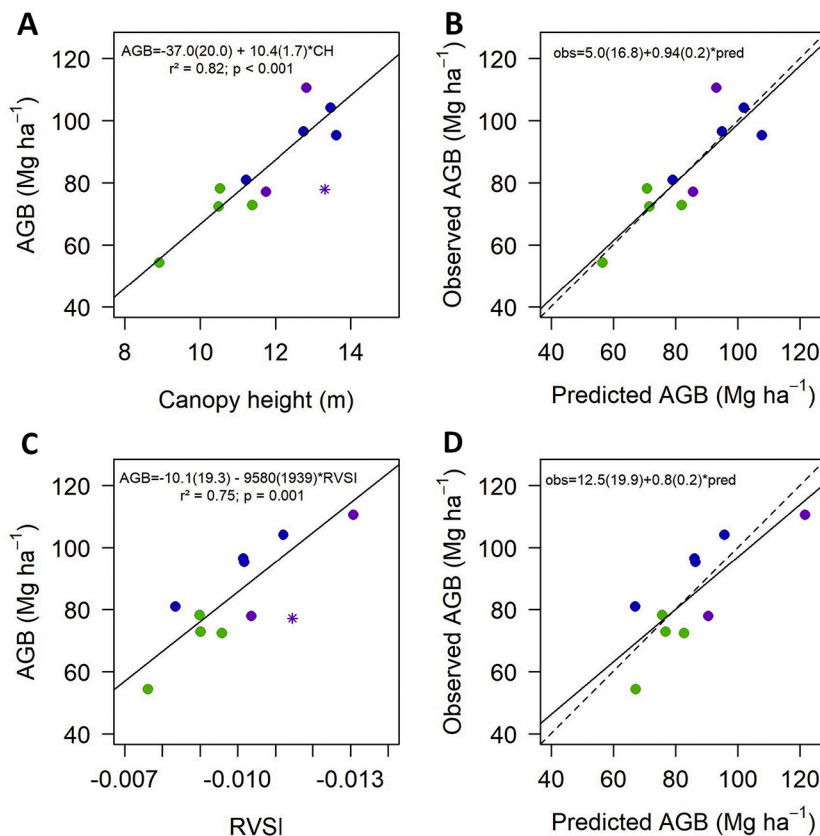

Fig. 6. Aboveground biomass of plots as a function of (A) lidar-derived canopy height (CH); and (C) hyperspectral-derived RVSI. The "*" purple point is an outlier plot not included in these regressions. Numbers in parentheses are the standard errors for each coefficient. (B) and (D) are Leave-one-out cross-validations (LOOCV) of aboveground biomass as a function of CH and RVSI, respectively. The dashed line represents a 1:1 correspondence, and the solid line is the linear regression fit between observed and leave-one-out predicted values ($obs_i = \alpha + \beta \cdot pred_i$). The values of α and β showed no significant difference from 0 and 1, respectively, in both cases. Point color represents the treatments of 20, 60, and 120 species (green, blue and purple, respectively). (For interpretation of the references to color in this figure legend, the reader is referred to the web version of this article.)

VARI using the ratios between the green (~ 550 nm) and red (~ 650 nm) bands and the CRI using two different green bands (~ 500 nm) (Gitelson et al., 2002, 2007). VARI has been proposed as a substitute for NDVI to measure canopy structure using ordinary RGB images (Fuentes-Peailillo et al., 2018; Gitelson et al., 2002). Among the structural VIs, EVI is known to have lesser degree of saturation with increasing LAI due to its higher sensitivity to NIR reflectance (non-saturated) than red reflectance, making it more responsive to canopy structural variations than indices such as NDVI (e.g. Huete et al., 2002). However, in our study EVI showed saturation at LAI = 2.0. Our analysis was conducted on an unprecedented fine spatial scale, allowing a better understanding of the relationship between the LAI and the VIs derived from high-spatial-resolution optical sensors, without the confounding effects of leaf age or sub-pixel shade fraction. Nevertheless, relationships (including VIs saturation) may be dependent on season and spatial resolution, an important question for future UAV-based high-resolution analysis that must be answered to connect UAV observations to those from coarser grain airborne and orbital sensors. We also note that the lidar-derived LAI represents a proxy for the actual LAI (Almeida et al., 2019a) and includes surface area contributions from other canopy components such as branches.

As expected, no HSI-derived variable was correlated to the understory LAI since HSI data are limited to the canopy surface, as is usual for optical sensors. On the other hand, lidar can record understory vegetation, providing information for forest restoration monitoring. The understory LAI showed potential to distinguish forest succession stages and forest types (Almeida et al., 2019a; Almeida et al., 2020a). Almeida et al. (2020a, 2020b), using a UAV-lidar system, showed that forest age was negatively correlated with understory LAI.

Some structural VIs were less spatially heterogeneous in the plots with higher LAI values (and higher richness levels). The saturation effect, in those cases, decreased their spatial heterogeneity, limiting the effectiveness of methods based on the spatial variation of VIs for estimating tree species diversity or the separation of forest types. VIs are limited in distinguishing between secondary and primary growth forests. However, using multiangular, off-nadir viewing hyperspectral data can improve forest successional stage discrimination (Galvão et al., 2009; Garcia Millan and Sanchez-Azofeifa, 2018). Combining temporal VIs analyses of land cover (vegetation or exposed soil) allows the determination of cover classes such as forest regeneration (including forest age) or short-term agricultural crop (Silva Junior et al., 2020).

The restoration plantations that we studied have a more homogenous canopy structure when compared with sites under natural regeneration, likely related to the even-aged cohort that comprises the canopy layer. We expect heterogeneity to increase with time through stand development competitive thinning dynamics, enhanced potentially by the years-to-decades that some slow-growing tropical trees require to express their unique structural characteristics and profile in the canopy. We believe that the ability of lidar technology to differentiate tree diversity levels may improve along with the structural development of forest stands. Conversely, the HSI spatial patterns were relevant proxies for distinguishing tree diversity levels even in 13-year-old restoration, highlighting the potential of this technology to monitor broad-scale restoration programs.

4.2. Distinguishing tree species richness levels

Several lidar-derived variables were more sensitive to differences in diversity than AGB. While we detected differences in AGB only between the treatments with 20 and 60 sp., LAI differed among all three diversity treatments and increased with each increasing species richness level. For the same study site, Duarte et al. (2021) found that AGB saturated from 60 sp. to 120 sp. while LAI and light interception (both derived from LAI-2200C equipment) were positively correlated to diversity even at very high richness levels. However, both our and Duarte et al. study evaluated only stem AGB and did not consider branches and leaves. Our

results also showed that canopy height was positively associated with species richness. Previous studies have shown that enhanced light interception and LAI in diverse tropical forests result from enhanced complementarity among crowns in canopy space, promoted by a high diversity of crown shapes and heights among species and neighborhood-driven plasticity in crowns (Guillemot et al., 2020; Duarte et al., 2021; Williams et al., 2017). We showed that the diversity effects on stand structure and AGB were efficiently captured by lidar-derived variables, which open promising perspectives for the large-scale monitoring of hyper-diverse tropical forest functioning. Canopy height heterogeneity and the LAI under the canopy did not significantly vary among treatments, which may be explained by the forest's low maturity and structural homogeneity. Increasing diversity and associated LAI in the upper canopy do not appear to impact understory LAI. A potential explanation for this surprising result is that light use efficiency increases with diversity—an expectation of higher crown type diversity—such that understory light availability changes little over this diversity gradient.

Structural VIs were positively associated with species richness. The capacity of VIs to discriminate among richness levels can be explained by the relatively low LAI compared with natural regeneration and mature forests (Almeida et al., 2019a). However, increasing LAI may result in saturation of the structural VIs and reduced ability to differentiate among richness levels. In general, the VIs that showed a significant difference among the treatments also showed an association with the canopy structure (i.e., significant correlation with LAI). It is important to note that many of the biochemical VIs were developed from laboratory spectrometers characterized by a higher signal-to-noise ratio (Meneses et al., 2019). The aerial collection of hyperspectral images (e.g. from drones) is subject to interference from the conditions of acquisition (atmospheric properties, geometry of acquisition) and canopy structure. However, some studies have shown promising results from VIs for tropical tree species classification (Ferreira et al., 2016).

One of the most interesting results concerning HSI data was that spectral diversity appeared to increase with richness treatments. The spectral angle was significantly different across categorical classes of species richness at $p < 0.1$ (Tukey test) and at $p < 0.05$ when species richness was treated as a continuous predictor in a simple linear regression (Table S2). The hyperspectral composition variable (MNF.1) differed among treatments in both mean and variance, and the spectral response showed higher variability in treatments with greater diversity (Fig. 5). By computing the spectral angle among the treatments, we showed that the spectral variability increased with diversity, which broadly agrees with the spectral variation hypothesis (Palmer et al., 2002). This hypothesis states that the spectral heterogeneity is induced by variations in habitat and has been used to assess forest canopy diversity with hyperspectral data (Féret and Asner, 2014). Our results suggested that tree diversity itself impacts spectral heterogeneity.

4.3. Predicting aboveground biomass

Some lidar and HSI variables demonstrated a remarkable capacity to estimate AGB accurately. This prediction represents a well-known potential of lidar structural data but is a less-universal finding for HSI variables. While VIs are known to saturate at high biomass and LAI values, the low plot-level density of vegetation (LAI ~ 2) in our study maintained VIs in an unsaturated range, where there is a strong correlation with AGB. This non-saturated stage behavior was also found in another study focusing on young, low diversity plantations established in a temperate forest ecosystem (Williams et al., 2021). The RVSI (Red-edge Vegetation Stress Index) was the most accurate predictor for biomass, which can be explained by the high positive correlation between the red-edge region (680–750 nm), the chlorophyll content, and the canopy LAI (Filella & Penuelas, 1994). The increase in the chlorophyll content tends to move the red-edge position to longer wavelengths, while the increase in LAI increases the difference between NIR and red reflectance. As the RVSI uses bands near the end of the red edge

(>730 nm), it may be sensitive to AGB variations induced by LAI and chlorophyll content.

The AGB predictions performed by the structural attribute derived from lidar (canopy height) did better than that of HSI-derived VIs. Lidar sensors have been shown to be the best tool for AGB estimates, especially in dense tropical rainforests (Wulder et al., 2012). Adding more variables to the model (multiple regression models) did not improve the prediction, probably due to the low structural complexity and low age of the vegetation. In a previous study performed in the same region but based on a greater number of forest types and more structurally complex forests, the addition of more variables improved AGB models (Almeida et al., 2019a). The utility of fusing lidar and hyperspectral data for AGB prediction per se remains an unresolved problem in the literature. Some studies have shown slight improvement with the addition of hyperspectral metrics in the AGB estimation models when they already have included lidar metrics (e.g. Clark et al., 2011; Fassnacht et al., 2014), while others have found better performance mixing lidar and HSI variables (e.g. Almeida et al., 2019b; Vaglio Laurin et al., 2014).

The use of lidar data as an intermediary layer between field and spectral satellite data ("upscaling" technique) is critical to generate large samples of AGB with high accuracy and thus generate more robust maps using satellite images for more extensive areas. Csillik et al. (2019) combined lidar and high-resolution satellite images to generate a biomass map for the entire country of Peru. New orbital lidar sensors are expected to generate more accurate maps of tropical forest AGB and stand structure attributes. One of them is the "Global Ecosystem Dynamics Investigation" (GEDI) orbital lidar sensor; however, its information is not spatially continuous and has much lower precision and accuracy compared with lidar sensors onboard aircraft and UAVs (Dubayah et al., 2020).

4.4. Monitoring tropical forest restoration

Given the high cost of field inventories, restoration programs have often used an insufficient number of plots, which have ultimately compromised the reliability of restoration field assessments (Viani et al., 2018). Upscaling restoration monitoring requires more than the replication over space of traditional forest inventory approaches because of the costs and scales involved (Brancalion and van Melis, 2017). At the other extreme, satellite images and novel analytical approaches are still incapable of measuring restoration quality (Rosa et al., 2021). A successful monitoring program must consider the gap between detailed and costly information from field plots and the million hectares of information generated by satellites with low capacity to detect restoration success.

We believe that the novel UAV-borne lidar and hyperspectral system described here can fill this technological gap, offering data streams that can be connected with plot-based monitoring and broad-scale remote sensing alike to improve upscaling and forest restoration monitoring. Particularly by blending lidar and HSI data, it is possible to assess biomass structural, functional, and diversity linked restoration outcomes simultaneously, a great advantage over methods based solely on either lidar or HSI. Further, it may represent a revolution in tracking restoration success globally. The development of new remote sensing approaches and their application to a restoration context would help expand our capacity to assess restoration over unprecedented spatial and temporal scales (White et al., 2019). Lidar-HSI upscaling has recently become possible due to the new generation of orbital sensors. In addition to the abovementioned spaceborne GEDI lidar mission, the DESIS (Krutz et al., 2019) and PRISMA (Vangi et al., 2021) hyperspectral sensors provide data with fine sampling using narrow bands (lower than 10 nm) and 30 m of spatial resolution. Together GEDI and DESIS or PRISMA data can provide unprecedented results on the structure and diversity of forest restoration at broader spatial scales. UAV-lidar-HSI systems are still relatively expensive and potentially unaffordable by some decision-making organizations such as governments, NGOs, small landowners, and companies.

In addition to acquisition costs, a high level of technical knowledge is required to operate drone-based systems and process and analyze the data. Thus, their use is still constrained to a minority of research groups. In tropical countries, particularly, the use of these systems is considerably limited due to high import tariffs and a lack of local technical assistance. However, these initial constraints are precisely the same faced by other technological innovations of the past, which are now broadly present in modern societies worldwide. Despite the constraints, efficient and relatively inexpensive UAV-lidar systems have been developed (Hu et al., 2020), which may facilitate their broader use in diverse sectors, particularly in forest restoration. Institutions in tropical countries should encourage the development of these technologies through investing in research, eliminating import taxes, encouraging open hardware development (Tsanni, 2020) and facilitating the arrival of specialized companies.

There are many benefits that UAV-lidar-HSI systems bring to forest restoration monitoring, including the potential to monitor small areas with very high accuracy, reduced field sampling effort (de Papa et al., 2020), and the increase of remote sampling for upscaling and generation of global models. Standardized monitoring protocols would help to evaluate restoration strategies' efficacy and compare results across projects to learn from the past and inform future restoration efforts (Viani et al., 2018). The unprecedented scale of global forest restoration targets will need to be accompanied by the evolution of restoration monitoring approaches and delivering, at much-reduced costs and higher spatial and temporal scales, critical information for tracking restoration success and guiding adaptive management. This constitutes an enormous scientific and technological challenge that has just started to be addressed by a joint effort of restoration, policymakers, and remote sensing experts. The positive results obtained by the UAV-lidar-HSI system described here are very encouraging and may hopefully foster the ongoing development and application of remote sensing innovations in ecosystem restoration.

Declaration of Competing Interest

The authors declare that they have no known competing financial interests or personal relationships that could have appeared to influence the work reported in this paper.

Acknowledgments

Appendix A. Supplementary data

Supplementary data to this article can be found online at https://doi.org/10.1016/j.rse.2021.112582.

References

Adhikari, H., Valbuena, R., Pellikka, P.K.E., Heiskanen, J., 2020. Mapping forest structural heterogeneity of tropical montane forest remnants from airborne laser scanning and Landsat time series. Ecol. Indic. 108, 105739.

Ali, A., Lin, S.-L., He, J.-K., Kong, F.-M., Yu, J.-H., Jiang, H.-S., 2019. Climate and soils determine aboveground biomass indirectly via species diversity and stand structural complexity in tropical forests. For. Ecol. Manag. 432, 823–831.

Almeida, D.R.A., Stark, S.C., Chazdon, R., Nelson, B.W., Cesar, R.G., Meli, P., Gorgens, E. B., Duarte, M.M., Valbuena, R., Moreno, V.S., Mendes, A.F., Amazonas, N., Gonçalves, N.B., Silva, C.A., Schietti, J., Brancalion, P.H.S., 2019a. The effectiveness of lidar remote sensing for monitoring forest cover attributes and landscape restoration. For. Ecol. Manag. 438, 34–43.

Almeida, D.R.A., Broadbent, E.N., Zambrano, A.M.A., Wilkinson, B.E., Ferreira, M.E., Chazdon, R., Meli, P., Gorgens, E.B., Silva, C.A., Stark, S.C., Valbuena, R., Papa, D.A., Brancalion, P.H.S., 2019b. Monitoring the structure of forest restoration plantations with a drone-lidar system. Int. J. Appl. Earth Obs. Geoinf. 79, 192–198.

Almeida, D.R.A., Stark, S.C., Silva, C.A., Hamamura, C., Valbuena, R., 2019c. leafR: Calculates the Leaf Area Index (LAD) and Other Related Functions. R package version 0.3. https://CRAN.R-project.org/package=leafR.

Almeida, D.R.A., Stark, S.C., Shao, G., Schietti, J., Nelson, B.W., Silva, C.A., Gorgens, E. B., Valbuena, R., de Papa, D.A., Brancalion, P.H.S., 2019a. Optimizing the remote detection of tropical rainforest structure with airborne lidar: leaf area profile sensitivity to pulse density and spatial sampling. Remote Sens. 11, 92.

Almeida, C.T., Galvão, L.S., de Aragão, L.E.O.C., Ometto, J.P.H.B., Jacon, A.D., de Pereira, F.R.S., Sato, L.Y., Lopes, A.P., de Graça, P.M.L.A., de Silva, C.V.J., Ferreira-Ferreira, J., Longo, M., 2019b. Combining LiDAR and hyperspectral data for aboveground biomass modeling in the Brazilian Amazon using different regression algorithms. Remote Sens. Environ. 232, 111323.

Almeida, D.R.A., Almeyda Zambrano, A.M., Broadbent, E.N., Wendt, A.L., Foster, P., Wilkinson, B.E., Salk, C., de Papa, D.A., Stark, S.C., Valbuena, R., Gorgens, E.B., Silva, C.A., Brancalion, P.H.S., Fagan, M., Meli, P., Chazdon, R., 2020a. Detecting successional changes in tropical forest structure using GatorEye drone-borne lidar. Biotropica 52, 1155–1167.

Almeida, D.R.A., Stark, S.C., Valbuena, R., Broadbent, E.N., Silva, T.S.F., Resende, A.F., Ferreira, M.P., Cardil, A., Silva, C.A., Amazonas, N., Zambrano, A.M.A., Brancalion, P.H.S., 2020b. A new era in forest restoration monitoring. Restor. Ecol. 28 (1), 8–11.

Amaral, C.H., de Almeida, T.I.R., de Souza Filho, C.R., Roberts, D.A., Fraser, S.J., Alves, M.N., Botelho, M., 2018. Characterization of indicator tree species in neotropical environments and implications for geological mapping. Remote Sens. Environ. 216, 385–400.

Asner, G.P., 2015. Organismic remote sensing for tropical forest ecology and conservation. Ann. Mo. Bot. Gard. 100, 127–140.

Asner, G.P., Martin, R.E., 2009. Airborne spectranomics: mapping canopy chemical and taxonomic diversity in tropical forests. Front. Ecol. Environ. 7, 269–276.

Asner, G.P., Martin, R.E., Knapp, D.E., Tupayachi, R., Anderson, C.B., Sinca, F., Vaughn, N.R., Llactayo, W., 2017. Airborne laser-guided imaging spectroscopy to map forest trait diversity and guide conservation. Science 355, 385–389.

Brancalion, P.H.S., Holl, K.D., 2020. Guidance for successful tree planting initiatives. J. Appl. Ecol. 57 (12), 2349–2361.

Brancalion, P.H.S., van Melis, J., 2017. On the need for innovation in ecological restoration. Ann. Mo. Bot. Gard. 102, 227–236.

Broadbent, E.N., Zambrano, A.M.A., Omans, G., Adler, A., Alonso, P., Naylor, D., Chenevert, G., Murtha, T., Vogel, J., Almeida, D.R.A., Dalla Corte, A.P., Silva, C.A., Prata, G.A., Merrick, T., D'Oliveira, M.V.N., Detto, M., Ferreira, M.P., Wilkinson, B. E., Ferreira, M.E., Landau, H.M., 2021. The GatorEye Unmanned Flying Laboratory: Sensor Fusion for 4D Ecological Analysis Through Custom Hardware and Algorithm Integration. http://www.speclab.org/gatoreye.html.

Camarretta, N., Harrison, P.A., Bailey, T., Potts, B., Lucieer, A., Davidson, N., Hunt, M., 2020. Monitoring forest structure to guide adaptive management of forest restoration: a review of remote sensing approaches. New For. 51, 573–596.

Chagas, G., Salk, C.F., Vidal, E.J., Souza, S.E.X.F., Brancalion, P.H.S., 2021. Exploiting fruits of a threatened palm to trigger restoration of Brazil's Atlantic Forest. Restor. Ecol. 29.

Clark, M.L., Roberts, D.A., Ewel, J.J., Clark, D.B., 2011. Estimation of tropical rain forest aboveground biomass with small-footprint lidar and hyperspectral sensors. Remote Sens. Environ. 115, 2931–2942.

Crouzeilles, R., Santiami, E., Rosa, M., Pugliese, L., Brancalion, P.H.S., Rodrigues, R.R., Metzger, J.P., Calmon, M., de Scaramuzza, C.A.M., Matsumoto, M.H., Padovezi, A., de Benini, R.M., Chaves, R.B., Metzker, T., Fernandes, R.B., Scarano, F.R., Schmitt, J., Lui, G., Christ, P., Vieira, R.M., Pinto, S., 2019. There is hope for achieving ambitious Atlantic Forest restoration commitments. Perspect. Ecol. Conserv. 17, 80–83.

Csillik, O., Kumar, P., Mascaro, J., O'Shea, T., Asner, G.P., 2019. Monitoring tropical forest carbon stocks and emissions using Planet satellite data. Sci. Rep. 9 (1), 1–12.

da Costa, V.A.M., da Oliveira, A.F., dos Santos, J.G., Bovo, A.A.A., de Almeida, D.R.A., Gorgens, E.B., 2020. Assessing the utility of airborne laser scanning derived indicators for tropical forest management. Southern For. 82, 352–358.

Dalagnol, R., Wagner, F.H., Galvão, L.S., Streher, A.S., Phillips, O.L., Gloor, E., Pugh, T.A. M., Ometto, J.P.H.B., Aragão, L.E.O.C., 2021. Large-scale variations in the dynamics of Amazon forest canopy gaps from airborne lidar data and opportunities for tree mortality estimates. Sci. Rep. 11, 1388.

Dalla Corte, A.P., Rex, F.E., de Almeida, D.R.A., Sanquetta, C.R., Silva, C.A., Moura, M. M., Wilkinson, B., Zambrano, A.M.A., da Cunha Neto, E.M., Veras, H.F.P., de Moraes, A., Klauberg, C., Mohan, M., Cardil, A., Broadbent, E.N., 2020. Measuring individual tree diameter and height using GatorEye high-density UAV-lidar in an integrated crop-livestock-forest system. Remote Sens. 12, 863.

De Cáceres, M., Martín-Alcón, S., González-Olabarria, J.R., Coll, L., 2019. A general method for the classification of forest stands using species composition and vertical and horizontal structure. Ann. For. Sci. 76, 40.

de Papa, D.A., de Almeida, D.R.A., Silva, C.A., Figueiredo, E.O., Stark, S.C., Valbuena, R., Rodriguez, L.C.E., d'Oliveira, M.V.N., 2020. Evaluating tropical forest classification and field sampling stratification from lidar to reduce effort and enable landscape monitoring. For. Ecol. Manag. 457, 117634.

d'Oliveira, M.V.N., Broadbent, E.N., Oliveira, L.C., Almeida, D.R.A., Papa, D.A., Ferreira, M.E., Zambrano, A.M.A., Silva, C.A., Avino, F.S., Prata, G.A., Mello, R.A., Figueiredo, E.O., de Jorge, L.A.C., Junior, L., Albuquerque, R.W., Brancalion, P.H.S., Wilkinson, B., Oliveira-da-Costa, M., 2020. Aboveground biomass estimation in Amazonian tropical forests: a comparison of aircraft- and GatorEye UAV-borne LiDAR data in the Chico Mendes Extractive Reserve in Acre, Brazil. Remote Sens. 12, 1754.

Duarte, M.M., Moral, R.A., Guillemot, J., Isaac, C., Zuim, F., Potvin, C., Bonat, W.H., Stape, J.L., Brancalion, P.H.S., 2021. High tree diversity enhances light interception in tropical forests. J. Ecol. 109 (7), 2597–2611.

Dubayah, R., Blair, J.B., Goetz, S., Fatoyinbo, L., Hansen, M., Healey, S., Hofton, M., Hurtt, G., Kellner, J., Luthcke, S., Armston, J., Tang, H., Duncanson, L., Hancock, S., Jantz, P., Marselis, S., Patterson, P.L., Qi, W., Silva, C., 2020. The global ecosystem dynamics investigation: high-resolution laser ranging of the Earth's forests and topography. Sci. Remote Sens. 1, 100002.

Erbaugh, J.T., Oldekop, J.A., 2018. Forest landscape restoration for livelihoods and well-being. Curr. Opin. Sustain. 32, 76–83.

Fagan, M.E., Reid, J.L., Holland, M.B., Drew, J.G., Zahawi, R.A., 2020. How feasible are global forest restoration commitments? Conserv. Lett. 13 (3), e12700.

Fassnacht, F.E., Hartig, F., Latifi, H., Berger, C., Hernández, J., Corvalán, P., Koch, B., 2014. Importance of sample size, data type and prediction method for remote sensing-based estimations of aboveground forest biomass. Remote Sens. Environ. 154, 102–114.

Feret, J.-B., Asner, G.P., 2013. Tree species discrimination in tropical forests using airborne imaging spectroscopy. IEEE Trans. Geosci. Remote Sens. 51, 73–84.

Féret, J.-B., Asner, G.P., 2014. Mapping tropical forest canopy diversity using high-fidelity imaging spectroscopy. Ecol. Appl. 24, 1289–1296.

Ferez, A.P., 2012. Efeito de práticas silviculturais sobre as taxas iniciais de sequestro de carbono em plantios de restauração da Mata Atlântica. Master thesis. Universidade de São Paulo, Piracicaba, São Paulo, Brazil, p. 104.

Ferez, A.P.C., Campoe, O.C., Mendes, J.C.T., Stape, J.L., 2015. Silvicultural opportunities for increasing carbon stock in restoration of Atlantic forests in Brazil. For. Ecol. Manag. 350, 40–45.

Ferreira, M.P., Zortea, M., Zanotta, D.C., Shimabukuro, Y.E., de Souza Filho, C.R., 2016. Mapping tree species in tropical seasonal semi-deciduous forests with hyperspectral and multispectral data. Remote Sens. Environ. 179, 66–78.

Ferreira, M.P., Féret, J.-B., Grau, E., Gastellu-Etchegorry, J.-P., Shimabukuro, Y.E., de Souza Filho, C.R., 2018. Retrieving structural and chemical properties of individual tree crowns in a highly diverse tropical forest with 3D radiative transfer modeling and imaging spectroscopy. Remote Sens. Environ. 211, 276–291.

Ferreira, M.P., Wagner, F.H., Aragão, L.E.O.C., Shimabukuro, Y.E., de Souza Filho, C.R., 2019. Tree species classification in tropical forests using visible to shortwave infrared WorldView-3 images and texture analysis. ISPRS J. Photogramm. Remote Sens. 149, 119–131.

Ferreira, M.P., de Almeida, D.R.A., de Papa, D.A., Minervino, J.B.S., Veras, H.F.P., Formighieri, A., Santos, C.A.N., Ferreira, M.A.D., Figueiredo, E.O., Ferreira, E.J.L., 2020. Individual tree detection and species classification of Amazonian palms using UAV images and deep learning. For. Ecol. Manag. 475, 118397.

Filella, I., Penuelas, J., 1994. The red edge position and shape as indicators of plant chlorophyll content, biomass and hydric status. Int. J. Remote Sens. 15, 1459–1470.

Finegan, B., Peña-Claros, M., de Oliveira, A., Ascarrunz, N., Bret-Harte, M.S., Carreño-Rocabado, G., Casanoves, F., Díaz, S., Eguiguren Velepucha, P., Fernandez, F., Licona, J.C., Lorenzo, L., Salgado Negret, B., Vaz, M., Poorter, L., 2015. Does functional trait diversity predict above-ground biomass and productivity of tropical forests? Testing three alternative hypotheses. J. Ecol. 103, 191–201.

Fox, J., Weisberg, S., 2019. An R Companion to Applied Regression, 3rd ed. Sage, Thousand Oaks CA. Retrieved from. https://socialsciences.mcmaster.ca/jfox/Books/Companion/.

Fuentes-Peailillo, F., Ortega-Farias, S., Rivera, M., Bardeen, M., Moreno, M., 2018. Comparison of vegetation indices acquired from RGB and multispectral sensors placed on UAV. In: 2018 IEEE International Conference on Automation/XXIII Congress of the Chilean Association of Automatic Control (ICA-ACCA). IEEE, pp. 1–6.

Galvão, L.S., Ponzoni, F.J., Liesenberg, V., dos Santos, J.R., 2009. Possibilities of discriminating tropical secondary succession in Amazônia using hyperspectral and multiangular CHRIS/PROBA data. Int. J. Appl. Earth Obs. Geoinf. 11, 8–14.

Gamfeldt, L., Snäll, T., Bagchi, R., Jonsson, M., Gustafsson, L., Kjellander, P., Ruiz-Jaen, M.C., Fröberg, M., Stendahl, J., Philipson, C.D., Mikusiński, G., Andersson, E.,

Westerlund, B., Andrén, H., Moberg, F., Moen, J., Bengtsson, J., 2013. Higher levels of multiple ecosystem services are found in forests with more tree species. Nat. Commun. 4, 1340.

Gamon, J.A., Serrano, L., Surfus, J.S., 1997. The photochemical reflectance index: an optical indicator of photosynthetic radiation use efficiency across species, functional types, and nutrient levels. Oecologia 112, 492–501.

Garcia Millan, V., Sanchez-Azofeifa, A., 2018. Quantifying changes on Forest succession in a dry tropical Forest using angular-hyperspectral remote sensing. Remote Sens. 10, 1865.

Gitelson, A.A., Kaufman, Y.J., Stark, R., Rundquist, D., 2002. Novel algorithms for remote estimation of vegetation fraction. Remote Sens. Environ. 80, 76–87.

Gitelson, A.A., Keydan, G.P., Merzlyak, M.N., 2006. Three-band model for noninvasive estimation of chlorophyll, carotenoids, and anthocyanin contents in higher plant leaves. Geophys. Res. Lett. 33.

Gitelson, A.A., Zur, Y., Chivkunova, O.B., Merzlyak, M.N., 2007. Assessing carotenoid content in plant leaves with reflectance spectroscopy. Photochem. Photobiol. 75, 272–281.

Gonçalves, N.B., Lopes, A.P., Dalagnol, R., Wu, J., Pinho, D.M., Nelson, B.W., 2020. Both near-surface and satellite remote sensing confirm drought legacy effect on tropical forest leaf phenology after 2015/2016 ENSO drought. Remote Sens. Environ. 237, 111489.

Green, A.A., Berman, M., Switzer, P., Craig, M.D., 1988. A transformation for ordering multispectral data in terms of image quality with implications for noise removal. IEEE Trans. Geosci. Remote Sens. 26, 65–74.

Guariguata, M.R., Evans, K., 2020. A diagnostic for collaborative monitoring in forest landscape restoration. Restor. Ecol. 28, 742–749.

Guillemot, J., Kunz, M., Schnabel, F., Fichtner, A., Madsen, C.P., Gebauer, T., Härdtle, W., von Oheimb, G., Potvin, C., 2020. Neighbourhood-mediated shifts in tree biomass allocation drive overyielding in tropical species mixtures. New Phytol. 228, 1256–1268.

Hernández-Stefanoni, J., Dupuy, J., Johnson, K., Birdsey, R., Tun-Dzul, F., Peduzzi, A., Caamal-Sosa, J., Sánchez-Santos, G., López-Merlín, D., 2014. Improving species diversity and biomass estimates of tropical dry forests using airborne lidar. Remote Sens. 6, 4741–4763.

Höhl, M., Ahimbisibwe, V., Stanturf, J.A., Elsasser, P., Kleine, M., Bolte, A., 2020. Forest landscape restoration—what generates failure and success? Forests 11, 938.

Horler, D.N.H., Dockray, M., Barber, J., 1983. The red-edge of plant leaf reflectance. Int. J. Remote Sens. 4, 273–288.

Hu, T., Sun, X., Su, Y., Guan, H., Sun, Q., Kelly, M., Guo, Q., 2020. Development and performance evaluation of a very low-cost UAV-Lidar system for forestry applications. Remote Sens. 13, 77.

Huete, A., Didan, K., Miura, T., Rodriguez, E.P., Gao, X., Ferreira, L.G., 2002. Overview of the radiometric and biophysical performance of the MODIS vegetation indices. Remote Sens. Environ. 83, 195–213.

Isenburg, M., 2020. LAStools - Efficient LiDAR Processing Software (version 1.8, Licensed). Obtained from. http://rapidlasso.com/LAStools.

Jia, W., Pang, Y., Tortini, R., Schläpfer, D., Li, Z., Roujean, J.-L., 2020. A kernel-driven BRDF approach to correct airborne hyperspectral imagery over forested areas with rugged topography. Remote Sens. 12, 432.

Jordan, C.F., 1969. Derivation of leaf-area index from quality of light on the Forest floor. Ecology 50, 663.

Keil, P., Chase, J.M., 2019. Global patterns and drivers of tree diversity integrated across a continuum of spatial grains. Nat. Ecol. Evol. 3, 390–399.

Kim, M.S., 1994. The Use of Narrow Spectral Bands for Improving Remote Sensing Estimations of Fractionally Absorbed Photosynthetically Active Radiation. Digital Repository at the University of Maryland.

Kotivuori, E., Kukkonen, M., Mehtätalo, L., Maltamo, M., Korhonen, L., Packalen, P., 2020. Forest inventories for small areas using drone imagery without in-situ field measurements. Remote Sens. Environ. 237, 111404.

Krůček, M., Král, K., Cushman, K.C., Missarov, A., Kellner, J.R., 2020. Supervised segmentation of ultra-high-density drone Lidar for large-area mapping of individual trees. Remote Sens. 12, 3260.

Krutz, D., Müller, R., Knodt, U., Günther, B., Walter, I., Sebastian, I., Säuberlich, T., Reulke, R., Carmona, E., Eckardt, A., Venus, H., Fischer, C., Zender, B., Arloth, S., Lieder, M., Neidhardt, M., Grote, U., Schrandt, F., Gelmi, S., Wojtkowiak, A., 2019. The instrument design of the DLR earth sensing imaging spectrometer (DESIS). Sensors (Basel, Switzerland) 19.

Laliberté, E., Schweiger, A.K., Legendre, P., 2020. Partitioning plant spectral diversity into alpha and beta components. Ecol. Lett. 23, 370–380.

Lasky, J.R., Uriarte, M., Boukili, V.K., Erickson, D.L., John Kress, W., Chazdon, R.L., 2014. The relationship between tree biodiversity and biomass dynamics changes with tropical forest succession. Ecol. Lett. 17, 1158–1167.

Lin, Q., Huang, H., Wang, J., Huang, K., Liu, Y., 2019. Detection of Pine Shoot Beetle (PSB) stress on pine forests at individual tree level using UAV-based hyperspectral imagery and lidar. Remote Sens. 11, 2540.

MacArthur, R.H., Horn, H.S., 1969. Foliage profile by vertical measurements. Ecology 50, 802.

Marselis, S.M., Abernethy, K., Alonso, A., Armston, J., Baker, T.R., Bastin, J., Bogaert, J., Boyd, D.S., Boeckx, P., Burslem, D.F.R.P., Chazdon, R., Clark, D.B., Coomes, D., Duncanson, L., Hancock, S., Hill, R., Hopkinson, C., Kearsley, E., Kellner, J.R., Kenfack, D., Dubayah, R., 2020. Evaluating the potential of full-waveform lidar for mapping pan-tropical tree species richness. Glob. Ecol. Biogeogr. 29 (10), 1799–1816.

Meneses, P.R., de Almeida, T., de Mello Baptista, G.M., 2019. Reflectância dos materiais terrestres. Oficina de Textos.

Mensah, S., Salako, V.K., Seifert, T., 2020. Structural complexity and large-sized trees explain shifting species richness and carbon relationship across vegetation types. Funct. Ecol. 34 (8), 1731–1745.

Merton, R., Huntington, J.,1999. Early simulation results of the ARIES-1 satellite sensor for multi-temporal vegetation research derived from AVIRIS. Available at https://aviris.jpl.nasa.gov/proceedings/workshops/99_docs/41.pdf, NASA Jet Propulsion Lab., Pasadena, CA. (Accessed 07 July 2021).

Palmer, M.W., Earls, P.G., Hoagland, B.W., White, P.S., Wohlgemuth, T., 2002. Quantitative tools for perfecting species lists. Environmetrics (London, Ont.) 13, 121–137.

Peñuelas, J., Baret, F., Filella, I., 1995. Semiempirical indexes to assess carotenoids chlorophyll-a ratio from leaf spectral reflectance. Photosynthetica 31, 221–230.

Peñuelas, J., Pinol, J., Ogaya, R., Lilella, I., 1997. Estimation of plant water content by thereflectance water index WI (R900/R970). Int. J. Remote Sens. 18, 2869–2875.

Poorter, L., van der Sande, M.T., Thompson, J., Arets, E.J.M.M., Alarcón, A., Álvarez-Sánchez, J., Ascarrunz, N., Balvanera, P., Barajas-Guzmán, G., Boit, A., Bongers, F., Carvalho, F.A., Casanoves, F., Cornejo-Tenorio, G., Costa, F.R.C., de Castilho, C.V., Duivenvoorden, J.F., Dutrieux, L.P., Enquist, B.J., Fernández-Méndez, F., Peña-Claros, M., 2015. Diversity enhances carbon storage in tropical forests. Glob. Ecol. Biogeogr. 24, 1314–1328.

Prata, G.A., Broadbent, E.N., de Almeida, D.R.A., St. Peter, J., Drake, J., Medley, P., Corte, A.P.D., Vogel, J., Sharma, A., Silva, C.A., Zambrano, A.M.A., Valbuena, R., Wilkinson, B., 2020. Single-pass UAV-borne GatorEye LiDAR sampling as a rapid assessment method for surveying forest structure. Remote Sens. 12, 4111.

Price, J.C., 1994. How unique are spectral signatures? Remote Sens. Environ. 49, 181–186.

R Core Team, 2020. R: A Language and Environment for Statistical Computing. R Foundation for Statistical Computing website.

Richter, R., Reu, B., Wirth, C., Doktor, D., Vohland, M., 2016. The use of airborne hyperspectral data for tree species classification in a species-rich Central European forest area. Int. J. Appl. Earth Obs. Geoinf. 52, 464–474.

Rocchini, D., Balkenhol, N., Carter, G.A., Foody, G.M., Gillespie, T.W., He, K.S., Kark, S., Levin, N., Lucas, K., Luoto, M., Nagendra, H., Oldeland, J., Ricotta, C., Southworth, J., Neteler, M., 2010. Remotely sensed spectral heterogeneity as a proxy of species diversity: recent advances and open challenges. Ecol. Inform. 5, 318–329.

Rosa, M.R., Brancalion, P.H.S., Crouzeilles, R., Tambosi, L.R., Piffer, P.R., Lenti, F.E.B., Hirota, M., Santiami, E., Metzger, J.P., 2021. Hidden destruction of older forests threatens Brazil's Atlantic Forest and challenges restoration programs. Sci. Adv. 7.

Rouse, J.W., Haas, R.H., Schell, J.A., Deering, D.W., 1974. Monitoring vegetation systems in the Great Plains with ERTS. NASA Spec. Publ. 351, 309.

Roussel, J., Auty, D., 2019. lidR: Airborne LiDAR Data Manipulation and Visualization for Forestry Applications. R Package Version 2.0.0.

Sankey, T., Donager, J., McVay, J., Sankey, J.B., 2017. UAV lidar and hyperspectral fusion for forest monitoring in the southwestern USA. Remote Sens. Environ. 195, 30–43.

Silva Junior, C.H.L., Heinrich, V.H.A., Freire, A.T.G., Broggio, I.S., Rosan, T.M., Doblas, J., Anderson, L.O., Rousseau, G.X., Shimabukuro, Y.E., Silva, C.A., House, J. I., Aragão, L.E.O.C., 2020. Benchmark maps of 33 years of secondary forest age for Brazil. Sci. Data 7, 269.

Silva, C., Hudak, A., Vierling, L., Klauberg, C., Garcia, M., Ferraz, A., Keller, M., Eitel, J., Saatchi, S., 2017. Impacts of airborne lidar pulse density on estimating biomass stocks and changes in a selectively logged tropical forest. Remote Sens. 9, 1068.

Timothy, D., Onisimo, M., Riyad, I., 2016. Quantifying aboveground biomass in African environments: a review of the trade-offs between sensor estimation accuracy and costs. Trop. Ecol. 57 (3), 393–405.

Tsanni, A., 2020. African scientists leverage open hardware. Nature 582, 138.

Turner, D.P., Cohen, W.B., Kennedy, R.E., Fassnacht, K.S., Briggs, J.M., 1999. Relationships between leaf area index and landsat TM spectral vegetation indices across three temperate zone sites. Remote Sens. Environ. 70, 52–68.

Vaglio Laurin, G., Chen, Q., Lindsell, J.A., Coomes, D.A., Frate, F.D., Guerriero, L., Pirotti, F., Valentini, R., 2014. Above ground biomass estimation in an African tropical forest with lidar and hyperspectral data. ISPRS J. Photogramm. Remote Sens. 89, 49–58.

Vaglio Laurin, G., Puletti, N., Hawthorne, W., Liesenberg, V., Corona, P., Papale, D., Chen, Q., Valentini, R., 2016. Discrimination of tropical forest types, dominant species, and mapping of functional guilds by hyperspectral and simulated multispectral Sentinel-2 data. Remote Sens. Environ. 176, 163–176.

Valbuena, R., Hernando, A., Manzanera, J.A., Görgens, E.B., Almeida, D.R.A., Mauro, F., García-Abril, A., Coomes, D.A., 2017. Enhancing of accuracy assessment for forest above-ground biomass estimates obtained from remote sensing via hypothesis testing and overfitting evaluation. Ecol. Model. 366, 15–26.

Valbuena, R., O'Connor, B., Zellweger, F., Simonson, W., Vihervaara, P., Maltamo, M., Silva, C.A., Almeida, D.R.A., Danks, F., Morsdorf, F., Chirici, G., Lucas, R., Coomes, D.A., Coops, N.C., 2020. Standardizing ecosystem morphological traits from 3D information sources. Trends Ecol. Evol. 35, 656–667.

van den Berg, A.K., Perkins, T.D., 2005. Nondestructive estimation of anthocyanin content in autumn sugar maple leaves. HortScience 40, 685–686.

Vangi, E., D'Amico, G., Francini, S., Giannetti, F., Lasserre, B., Marchetti, M., Chirici, G., 2021. The new hyperspectral satellite PRISMA: imagery for forest types discrimination. Sensors (Basel, Switzerland) 21.

Versluijs, M., Hjältén, J., Roberge, J.-M., 2019. Ecological restoration modifies the value of biodiversity indicators in resident boreal forest birds. Ecol. Indic. 98, 104–111.

Viani, R.A.G., Barreto, T.E., Farah, F.T., Rodrigues, R.R., Brancalion, P.H.S., 2018. Monitoring young tropical forest restoration sites: how much to measure? Trop. Conserv. Sci. 11 (194008291878091).

Wanner, W., Li, X., Strahler, A.H., 1995. On the derivation of kernels for kernel-driven models of bidirectional reflectance. J. Geophys. Res. 100, 21077.

White, J.C., Wulder, M.A., Hermosilla, T., Coops, N.C., 2019. Satellite time series can guide forest restoration. Nature 569, 630.

Williams, L.J., Paquette, A., Cavender-Bares, J., Messier, C., Reich, P.B., 2017. Spatial complementarity in tree crowns explains overyielding in species mixtures. Nat. Ecol. Evol. 1, 63.

Williams, L.J., Cavender-Bares, J., Townsend, P.A., Couture, J.J., Wang, Z., Stefanski, A., Messier, C., Reich, P.B., 2021. Remote spectral detection of biodiversity effects on forest biomass. Nat. Ecol. Evol. 5, 46–54.

Wortley, L., Hero, J.-M., Howes, M., 2013. Evaluating ecological restoration success: a review of the literature. Restor. Ecol. 21, 537–543.

Wulder, M.A., White, J.C., Nelson, R.F., Næsset, E., Ørka, H.O., Coops, N.C., Hilker, T., Bater, C.W., Gobakken, T., 2012. Lidar sampling for large-area forest characterization: a review. Remote Sens. Environ. 121, 196–209.

Yan, J., Zhou, W., Han, L., Qian, Y., 2018. Mapping vegetation functional types in urban areas with WorldView-2 imagery: integrating object-based classification with phenology. Urban For. Urban Green. 31, 230–240.

Zellweger, F., Baltensweiler, A., Schleppi, P., Huber, M., Küchler, M., Ginzler, C., Jonas, T., 2019. Estimating below-canopy light regimes using airborne laser scanning: an application to plant community analysis. Ecol. Evol. 9, 9149–9159.

Zhao, Y., Zeng, Y., Zheng, Z., Dong, W., Zhao, D., Wu, B., Zhao, Q., 2018. Forest species diversity mapping using airborne LiDAR and hyperspectral data in a subtropical forest in China. Remote Sens. Environ. 213, 104–114.